

Form, function, and failure shape preferred flow paths in porous media

Emily Chen and Nitay Ben-Shachar*

Abstract Preferential flow paths arise in many network systems, from traffic networks to disease transmission and fluid flow in porous rock environments. Understanding why and how preferential flow paths form provides the basis for developing prediction methods to determine where and under what conditions preferred paths will occur, with direct application to forecasting natural landslide events, pathways of disease transmission, and predicting the fate of injected fluids in subsurface environments. This report provides a brief introduction to porous network models, prediction of flow paths based on discrete element simulations, landslide event and material fracture prediction, and introduces a toy mathematical model to predict landslide failure times.

1 Preferential flow paths in network systems

Preferential flow paths—or favoured routes—arise in numerous settings: optimised travel paths in traffic networks, channelisation of fluid flow within porous media, and pathways of transmission for communicable diseases. The focus of this section will be on understanding how we can find and predict these preferential flow paths for a given network using optimisation methods.

Emily Chen
Department of Chemical & Biological Engineering, Princeton University, USA
e-mail: ec2619@princeton.edu

Nitay Ben-Schachar
School of Mathematics & Statistics, University of Melbourne, Australia
e-mail: nbenshachar@student.unimelb.edu.au

* These lecture notes are based on the lectures delivered by Prof. Antoinette Tordesillas and Dr Edward Hinton (School of Mathematics and Statistics, University of Melbourne) at the Matrix Workshop *Instabilities in Porous Media*, April 3-23, 2024, who also assisted with the preparation of these notes.

One interesting example of predicting transmission networks is a study on the growth of slime mould towards systematically-placed food sources mirroring the rail network of the Tokyo metro system [2]. The resulting slime mould network structure mirrors that of the actual Tokyo rail system despite the mould not having any brain; these results suggest that disease transmission pathways may be predicted a priori for a given known network structure based on known locations of population centres.

1.1 Network flow theory

To understand how and why preferred flow paths form, we first construct a pore network model consisting of pore bodies and pore throats. The pore bodies are modelled by “nodes” and the pore throats are modelled by “edges”. Each edge is assigned a conductance or capacity for flow in addition to an edge cost, where the orientation of the edge relative to the bulk pressure gradient, ∇P , induces a misalignment penalty. A schematic of one example network is shown below in Fig. 1. The direction of arrows on each edge indicates the direction of flow along that edge, and the numerical value assigned to each edge corresponds to its capacity for flow.

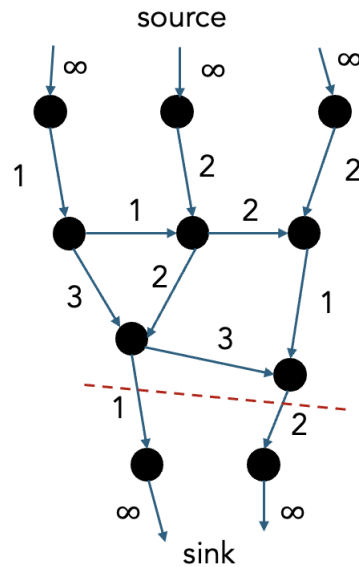


Fig. 1 Example pore network model. Black circles represent pore bodies, or nodes, and blue arrows indicate pore throats, or edges. The numerical values correspond to the capacitance of flow for each edge. The red dashed line shows the location of the edges comprising the minimum cut.

1.1.1 Maximum flow, minimum cut theorem

In graph theory, the minimum cut is the minimal sum of edge values where removing those selected edges would completely disconnect the source from the sink. The theorem of maximum flow, minimum cut states that the maximum amount of flow through the network is equivalent to the minimum cut. Physically, the edges comprising the minimum cut represent a “bottleneck” in the system that restricts the maximum amount of flow. In the example network above (Fig. 1), the minimum cut is indicated by the dashed red line, and the corresponding maximum flow through the system is 3.

1.2 Granular failure informatics and analytics

Granular media such as sand, rock packings, or loose soil exhibit dynamic restructuring under applied mechanical loads (e.g. compression, shearing, and tension). In some cases, failure of the granular matrix may occur, leading to drastic changes in the pore-scale and grain-scale morphologies. Methods such as digital image correlation (DIC), x-ray CT, and discrete element simulations (DEM) provide information on individual grain movement and displacement speeds during the applied mechanical load. One example of granular failure is the compression of an isotropic sand pack, where failure occurs due to the development of a high porosity shear band that thus enables the formation of preferential flow paths. Additionally, under compression, strandlike force chains between adjacent grains may develop. Large stresses propagate along these force chains, resulting in a highly heterogeneous distribution of forces within the granular material. Another feature exhibited by some granular materials under compression is a feature known as dilatancy: a bulk increase in volume that increases the medium permeability even before the onset of failure.

Data from experimental and simulation methods on the response of granular materials to mechanical loads can be used in machine learning algorithms to classify and predict members of preferred pathways by transforming the grain-scale data into a pore network framework. The required inputs into the algorithm are a discrete element model of the granular assembly with known edge capacitances and costs (Fig. 2). The machine learning algorithm can help to classify edges into three types: (1) primary edges—primary pathways for fluid flow, removal of these edges would stop flow entirely, (2) secondary edges—these edges serve as connections between primary flow paths and are typically oriented transversely to the main flow direction, and (3) tertiary edges—connecting edges with much smaller magnitudes of flow [5].

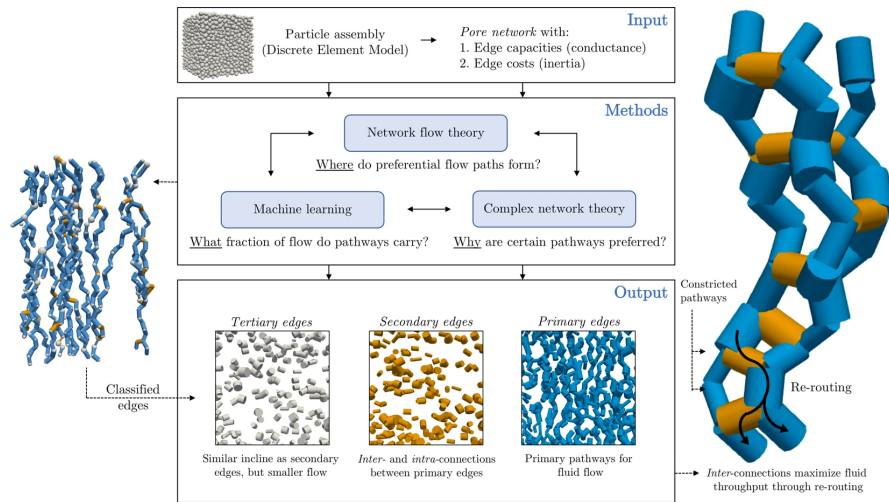


Fig. 2 Workflow of edge classification. Figure reproduced from [5].

1.2.1 Closeness centrality

Closeness centrality is a metric in graph theory that describes how “close” a node is to other nodes in the network. Nodes with high closeness centrality can transmit information more rapidly to other nodes in the network. Closeness centrality is calculated as the inverse of the sum of the distance from a node to all other nodes in the network.

2 Landslide mitigation

Landslides are a major hazard in regions with steep terrains and seasons of prolonged rainfall; the objective of landslide mitigation is to accurately forecast and predict failure events using real time ground motion monitoring from satellite systems and line-of-sight radars. These measurement systems monitor the movement of the ground surface, providing ground displacement data at a spatiotemporal resolution set by the measurement method. Data from actual failure events can be used to map out the network and provides statistics on where the instability develops. In particular, the closeness centrality metric shows the existence of highest centrality nodes located in a thin shear band connecting two larger clusters of nodes, where each of these clusters tends to move together. This network has a “bird-like” pattern where the failure zone is located at the nodes of highest closeness centrality. Further, data from before the failure event actually occurs can be used to predict the location of failure using the closeness centrality metric.

The method of approach to forecasting landslide formation first requires measurement of the cumulative displacement vectors of ground surface locations in x - y physical space. Next, converting from physical into kinematic phase space on a plot of u_x versus u_y and performing cluster analysis (e.g. K -means clustering) identifies ground surface regions that move most similar to each other. Additionally, the silhouette index measures the compactness and separateness of different clusters, and the Jaccard index measures the temporal persistence of each cluster. Replotting the identified clusters in x - y physical space reveals the prediction of the failure location even before the failure event occurs [3].

2.1 Toy model to predict the dynamics of landslides (E. Hinton)

The traditional model of creep, or the time-dependent deformation of a material under load, occurs in three stages. The first stage is primary creep, where the material resistance to deformation decreases with time ($\frac{d\varepsilon}{dt}$ decreases with time, where ε is material strain). Primary creep is followed by secondary creep which is a region of constant creep (nearly constant $\frac{d\varepsilon}{dt}$). In the final stage, tertiary creep, the deformation rate increases with time until material failure occurs ($\frac{d\varepsilon}{dt}$ increases with time).

Here, we treat the problem of rock detachment (failure event) as an analogue of a pendulum problem to predict the time to failure. Landslide locations are known to exhibit large displacements even before the failure event occurs, contrasting failure observed in perfectly brittle, rigid materials. The classical framework proposed by Voight [6] and Fukuzono [1] for the displacement is

$$\ddot{\Omega} = A\dot{\Omega}^\alpha, \quad (1)$$

where Ω is displacement, $\dot{\Omega}$ is velocity, $\ddot{\Omega}$ is acceleration, and A and α are fitting parameters. Integrating Eqn. (1) once and setting the integration constant as the time to failure, t_f , we obtain:

$$\dot{\Omega} = [(\alpha - 1)A(t_f - t)]^{-1/(\alpha-1)}. \quad (2)$$

Experimental studies suggest that the exponent α typically takes on values of 1.5-2.2. Figure 3(a) shows the plot of velocity versus time with a characteristic ‘‘hockey stick’’ profile, where the upturn indicates the failure event. Replotting the model as the inverse velocity versus time (Fig. 3(b)) allows for extraction of the failure time, t_f . This representation of failure behaviour recapitulates experimental velocity time series failure data from an actual landslide event fairly well (Fig. 3(d)). However, there is a large discrepancy between the model and experimental data when considering the phase plane of $\ddot{\Omega}$ versus $\dot{\Omega}$: experimental data show non-monotonic behaviour with a turning point in the acceleration (Fig. 3(e)), while the model only shows monotonic increase in acceleration with velocity. Another discrepancy is observed in the inverse velocity plots as the experimental data show a finite plateau

value (Fig. 3(f)) indicating a reduction in acceleration prior to failure not captured by the model. Thus, a modified model is necessary to account for the reduction in acceleration prior to failure. Here, we consider 3 inverted pendulum models to address this discrepancy: (1) simple inverted pendulum, (2) inverted pendulum with damping, and (3) elastic inverted pendulum.

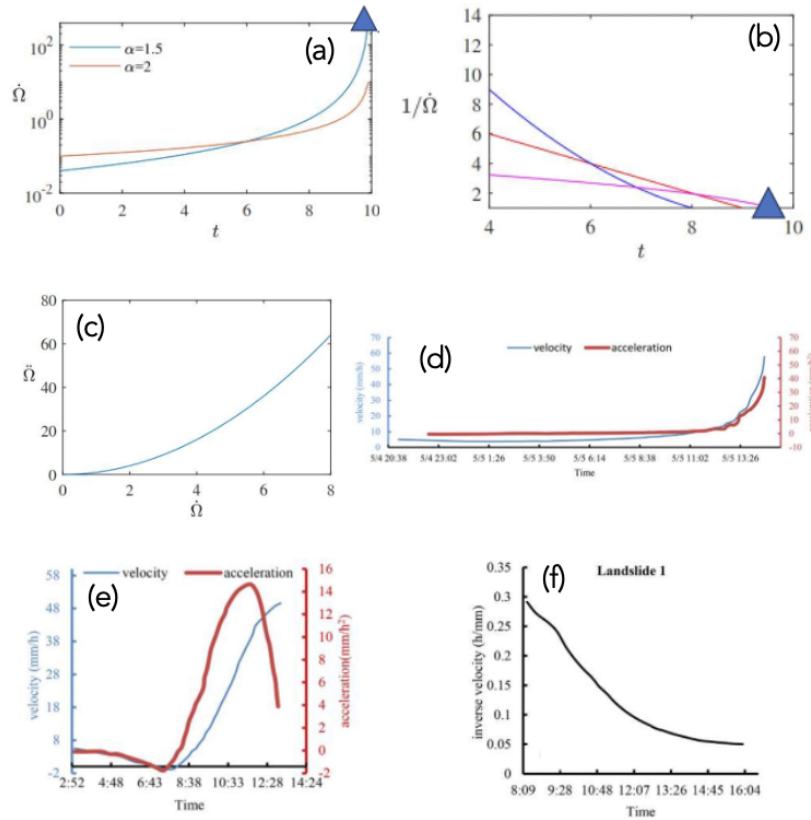


Fig. 3 Classical picture of creep failure. (a) Velocity versus time plot of Voigt and Fukuzono models [6, 1]. (b) Inverse velocity versus time plot of Voigt and Fukuzono models. (c) Phase plane of acceleration of speed given by of Voigt and Fukuzono models. (d) Experimental time series data of landslide from [7]. (e) Experimental time series data of landslide velocity and acceleration from [7]. (f) Experimental time series data of landslide inverse velocity from [7]. Figures in (d–f) are reproduced from [7].

The inverted pendulum is described by

$$\ddot{\theta} = \frac{g}{l} \sin \theta, \tag{3}$$

where g is gravitational acceleration, l is the length of the pendulum, and θ is the displacement angle. This system considers a mass located above a pivot point and is an unstable equilibrium.

The inverted pendulum with damping is described by

$$\ddot{\theta} = \frac{g}{l} \sin \theta - k\dot{\theta}^2, \quad (4)$$

where k is the damping coefficient. Proper selection of k can be used to fit the location of the peak in acceleration versus velocity to experimental data. Physically, damping may arise from friction within the granular material that stabilises the unstable equilibrium state.

The inverted pendulum with a spring is described by

$$\ddot{\theta} = \frac{1}{1+x} \sin \theta - \frac{2\dot{x}\dot{\theta}}{1+x}, \quad (5)$$

where $x = l\theta$ is the displacement of the spring and k is the spring constant. The ratio of the spring and pendulum frequencies is given by $\beta = \frac{\sqrt{k/m}}{\sqrt{g/l_0}}$. The spring term here mimics the physical “bonds” between rock grains. These models progressively build on a simplified toy model of the landslide event to improve upon the traditional model of creep by incorporating terms to account for physically relevant behaviours, such as friction and cohesive forces within the materials. The inclusion of physically-relevant terms better aligns with the experimental creep data from landslide events—specifically in capturing the reduction in acceleration prior to failure.

3 Fracture prediction

Network models can similarly be applied towards predicting failure in heterogeneous materials to identify locations and paths of fracturing. Using information from experimental mechanical tests and discrete element simulations, the material can be represented as a network with different bond strengths, forces, strain energies, and surface energies [4]. The fracture strength of each link in the network is given by the inverse of the relative motion of the edge, and comparison of adjacent edge strengths reveals the crack path from the bottleneck of “flow” in the material. Figure 4 shows a schematic of the prediction framework.

References

1. Fukozonu, T.: A new method for predicting the failure time of a slope failure. Proc. IVth Intl Conf and Field Workshop on Landslides (1985)

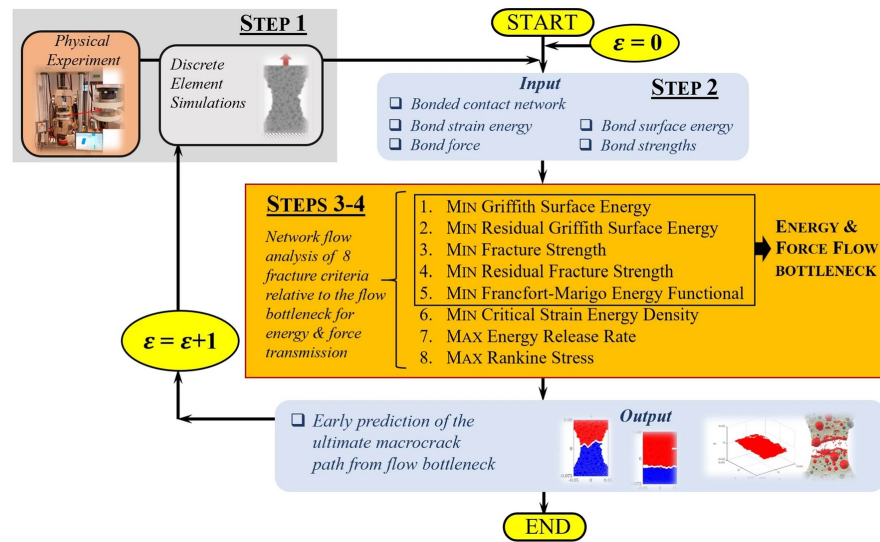


Fig. 4 Workflow of fracture prediction using network models. Reproduced from [4]

2. Tero, A., Takagi, S., Saigusa, T., Ito, K., Bebbler, D.P., Fricker, M.D., Yumiki, K., Kobayashi, R., Nakagaki, T.: Rules for Biologically Inspired Adaptive Network Design. *Science* **327**(5964), 439–442 (2010). DOI 10.1126/science.1177894. URL <https://www.science.org/doi/10.1126/science.1177894>
3. Tordesillas, A., Kahagalage, S., Campbell, L., Bellett, P., Intrieri, E., Batterham, R.: Spatiotemporal slope stability analytics for failure estimation (SSSAFE): linking radar data to the fundamental dynamics of granular failure. *Sci Rep* **11**(1), 9729 (2021). DOI 10.1038/s41598-021-88836-x. URL <https://www.nature.com/articles/s41598-021-88836-x>
4. Tordesillas, A., Kahagalage, S., Ras, C., Nitka, M., Tejchman, J.: Early prediction of macrocrack location in concrete, rocks and other granular composite materials. *Sci Rep* **10**(1), 20,268 (2020). DOI 10.1038/s41598-020-76616-y. URL <https://www.nature.com/articles/s41598-020-76616-y>
5. Van Der Linden, J.H., Tordesillas, A., Narsilio, G.A.: Preferential flow pathways in a deforming granular material: self-organization into functional groups for optimized global transport. *Sci Rep* **9**(1), 18,231 (2019). DOI 10.1038/s41598-019-54699-6. URL <https://www.nature.com/articles/s41598-019-54699-6>
6. Voight, B.: A method for prediction of volcanic eruptions. *Nature* **332**(6160), 125–130 (1988). DOI 10.1038/332125a0. URL <https://www.nature.com/articles/332125a0>
7. Zhou, X.P., Liu, L.J., Xu, C.: A modified inverse-velocity method for predicting the failure time of landslides. *Engineering Geology* **268**, 105,521 (2020). DOI 10.1016/j.enggeo.2020.105521. URL <https://linkinghub.elsevier.com/retrieve/pii/S001379521931751X>